evaluation of the primary loads acting on helicopter rotor blades," Giravios Dorand Rept. DE 2012(1960).

[3] Shi-Tsun, V., "The aerodynamic characteristics of a loaded helicopter rotor from a three-dimensional vortex system," Aviotsionnaya Tekhnika Number 1, transl. by M. A. P. Willmer, Royal Aircraft Establishment Library Translation 1013 (1961).

[4] Piziali, R. A. and DuWaldt, F. A., "Computation of rotary wing harmonic air loads and comparison with experimental results," *Proceedings of the American Helicopter Society Eighteenth Annual National Forum* (The American Helicopter Society, New York, 1962).

[5] Miller, R. H., "On the computation of air loads acting on rotor blades in forward flight," J. Am. Helicopter Soc. **7**, 235–254 (1962).

[6] Molyneux, W. G., "An approximate theoretical approach for the determination of oscillatory aerodynamic coefficients for a helicopter rotor in forward flight," Aeronaut. Quart., XIII, (August 1962).

[7] Piziali, R. A. and DuWaldt, F. A., "Computed induced velocity, induced drag, and angle of attack distribution for a two-bladed rotor," *Proceedings of the American Helicopter Society Nineteenth Annual National Forum* (The American Helicopter Society, New York, 1963).

[8] Miller, R. H., "Rotor blade harmonic air loading," AIAA J. **2**, 1254–1269 (1964).

[9] Miller, R. H., "Unsteady air loads on helicopter rotor blades," J. Roy. Aeronaut. Soc. **68**, 217–229 (1964).

[10] Davenport, F. J., "A method for computation of the induced velocity field of a rotor in forward flight, suitable for application to tandem rotor configurations," J. Am. Helicopter Soc. **9**, (1964).

[11] Harrison, J. M. and Ollerhead, J. B., "The nature of limitations imposed on the performance of a helicopter rotor," *Symposium on the Noise and Loading Actions on Helicopter V/STOL Aircraft and Ground Effect Machines*; also J. Sound Vibration (to be published).

[12] Piziali, R. A., "Method for solution of the aeroelastic response problems for rotating wings," Symposium on the Noise and Loading Actions on Helicopter V/STOL Aircraft and Ground Effect Machines; also J. Sound Vibration (to be published.)

[13] Piziali, R. A. and DuWaldt, F. A., "A method for computing rotary wing air load distribution in forward flight," Transportation Research Command Rept. TR-62-44 (November 1962).

[14] Gessow, A. and Crim, A. D., "A method for studying the transient blade-flapping behavior of lifting rotors at extreme operating conditions," National Advisory Committee for Aeronautics TN 3366 (January 1955).

[15] Scheiman, J. and Ludi, L. H., "Effect of helicopter rotor-blade tip vortex on blade air loads," NASA TN D-1637 (May 1963).

[16] Segel, L., "Air loadings on a rotor blade as caused by transient inputs of collective pitch," U. S. Army Aviation Labs., TR 65-65 (October 1965).

[17] Scheiman, J., "A tabulation of helicopter rotor-blade differential pressures, stresses, and motions as measured in flight," NASA TM X-952 (March 1964).

[18] Rabbott, J. P., Jr., "CH-34 Rotor Data," Sikorsky Aircraft Corp., personal communication (March 15, 1965).

[19] *Proceedings of CAL/TRECOM Symposium on Dynamic Problems Associated with Helicopters and V/STOL Aircraft* (Cornell Aeronautical Labs., Buffalo, N. Y., 1963).

NOV.-DEC. 1966 J. AIRCRAFT VOL. 3, NO. 6

Hypersonic Inlet Boundary-Layer Research

JOHN F. STROUD* AND LEONARD D. MILLER†
Lockheed-California Company, Burbank, Calif.

Recent results of a combined analytical and experimental hypersonic inlet boundary-layer research program are reviewed. New turbulent boundary-layer data with heat transfer are presented for a representative compression surface in the Mach number range of 5–8. Surface cooling is shown to have favorable effects on boundary-layer characteristics. The experimental data, with and without cooling, are correlated with a theory developed in this program. The theory has been applied to typical inlets to determine effects of heat transfer and centrifugal forces on basic boundary-layer characteristics as well as on over-all inlet pressure recovery. Both phenomena are favorable, resulting in improved inlet pressure recovery. Centrifugal force effects are more pronounced in low fineness ratio inlets whereas heat transfer effects tend to predominate in high fineness ratio inlets, wherein the supersonic compressive turning is more gradual.

Nomenclature

C_f = local skin friction
h = static enthalpy
H = shape parameter
H_e = shape parameter, δ_e^*/θ_e
H_w = shape parameter, δ_w^*/θ_w
H^1 = total enthalpy
H^* = total enthalpy parameter, $H^1 - h_w$
M = Mach number
P = pressure
q = dynamic pressure
T = temperature
R_e = Reynolds number
u = velocity component along x
u_1 = inviscid velocity component along x
v = velocity component along y
x = distance along surface of body
y = distance normal to body surface
γ = ratio of specific heats
δ = boundary-layer thickness
δ_e^* = displacement thickness, $\int_0 \left(1 - \frac{\rho u}{\rho_e u_e}\right)$ dynes
δ_w^* = displacement thickness, $\int_0^\delta \left(\frac{\rho_1 u_1}{\rho_{1_w} u_{1_w}} - \frac{\rho u}{\rho_{1_w} u_{1_w}}\right)$ dynes
θ_e = momentum thickness, $\int_0^\delta \frac{\rho u}{\rho_e u_e}\left(1 - \frac{u}{u_e}\right)$ dynes
θ_w = momentum thickness, $\int_0^\delta \frac{\rho u}{\rho_{1_w} u_{1_w}}\left(\frac{u_1}{u_{1_w}} - \frac{u}{u_{1_w}}\right)$ dynes

Presented as Preprint 65-605 at the AIAA Propulsion Joint Specialist Conference, Colorado Springs, Colo., June 14–18, 1965; submitted December 6, 1965; revision received June 13, 1966. This research was sponsored in part by the Air Force Flight Dynamics Laboratory, Research and Technology Division, under Contract AF 33(657)-8833 and Lockheed-California Company. R. L. Balent is the RTD Project Engineer.

* Propulsion Department Manager. Member AIAA.
† Research Specialist. Member AIAA.

ρ = density

ϕ = energy thickness, $\int_0^\delta \left(1 - \frac{H^*}{H_e{}^*}\right) \frac{\rho u}{\rho_e u_e}$ dynes

Subscripts

e = condition at the edge of boundary layer
o = freestream
t = stagnation conditions
w = conditions based on wall values
1 = inviscid flow
i = initial value

Introduction

ONE of the major problems associated with design of hypersonic airbreathing propulsion systems involves boundary-layer development in the inlet. This boundary-layer comprises a large portion of the inlet flow and is extremely complicated by virtue of the environment, including strong adverse pressure gradients, heat transfer, centrifugal forces and real gas effects. A knowledge of the boundary layer is necessary 1) to enable appropriate design compromises involving pressure recovery, drag, and weight to be made, and 2) to permit appropriate contour corrections to be incorporated for displacement effects in any given inlet design. Accordingly, the rational design of hypersonic systems requires understanding of the physical phenomena, as well as analytical methods for predicting the boundary layer in the complex environment of hypersonic inlets. Previous results of a combined experimental and analytical program having these goals are presented in Refs. 1 and 2. The purpose of the present paper is 1) to present recent experimental and analytical results, and 2) to provide examples of application of the theory developed in this program to hypersonic inlet design problems.

Experimental Program

Models and Tests

Four axially symmetric models were designed and built with reverse Prandtl-Meyer compression surfaces to provide continuous supersonic, shock free, external compression (Fig. 1). The compression surfaces are preceded by boundary-layer generating cylinders that include tripping devices for forcing transition. Hollow generating cylinders were used instead of pointed closed spikes (as in hypersonic inlets) to enable boundary layers of various thicknesses and profiles to be generated. The generating cylinders can be varied in length by a factor of about 3. Both the generating cylinders and compression surfaces are designed to permit air to flow through the entire model without choking. The four models designed for Mach 4, 5, 6, and 8 were sized for testing in Arnold Engineering Development Center (AEDC) Tunnels

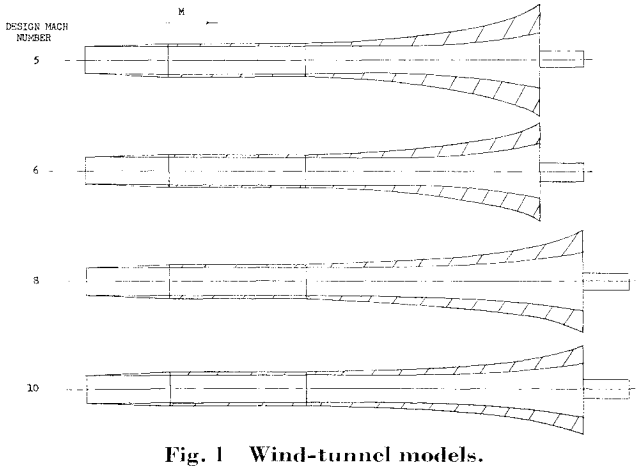

Fig. 1 Wind-tunnel models.

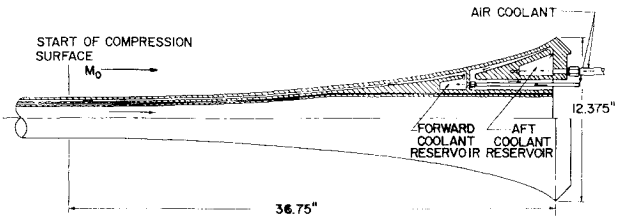

Fig. 2 Heat-transfer model.

A and B at Reynolds numbers comparable to full-scale inlet values. Each was tested at both design and off-design Mach numbers to obtain the effects of variation in rate of compression on boundary-layer characteristics.

The Mach 8 design has provisions for wall cooling, as shown in Fig. 2. The walls were cooled by means of pressurized air, which was first passed through coils in a tank of liquid nitrogen and then mixed with uncooled air. Finally, the cooled air was passed through the coolant passages of the model. Two independent cooling passages, one forward and one aft, were provided for the purpose of obtaining an isothermal wall. The need for two independent passages is dictated by the large difference in heat transfer in the forward and aft sections of the model. The cooled model is larger than the uncooled models in order to provide a wall thickness sufficiently large to permit heat-transfer measurements to be made. A photograph of the Mach 5 design compression surface with a 17-in boundary-layer generating cylinder attached is shown installed in Tunnel A in Fig. 3. The boundary-layer survey probes and mechanism are also shown in this photograph.

The models were tested at Mach numbers of 4, 5, 6, and 8 over a range of Reynolds numbers from 0.85×10^6–6.9×10^6/ft. Inasmuch as this program concentrated on the study of turbulent boundary layers, it was necessary to provide artificial transition on the boundary-layer generating cylinders ahead of the model compression surface. Of the various devices tested, including 1) wires normal to the surface, 2) air injection normal to the surface, and 3) vortex generators, the latter provided the thinnest and least distorted boundary-layer profile. Accordingly, vortex generators were used throughout the majority of the tests.

Instrumentation

Instrumentation was provided to measure surface temperature and pressure in addition to total pressure, static pressure, and total temperature at various distances from the surface in the boundary layer. Surface temperature and pressure measurements were made at numerous streamwise stations, with the spacing being closer at the downstream end

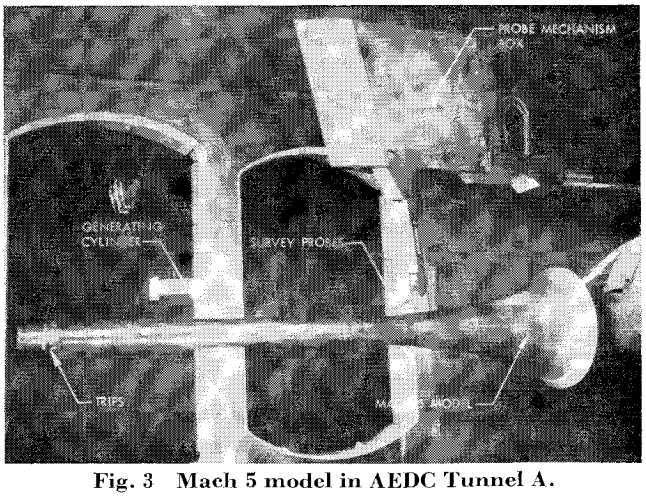

Fig. 3 Mach 5 model in AEDC Tunnel A.

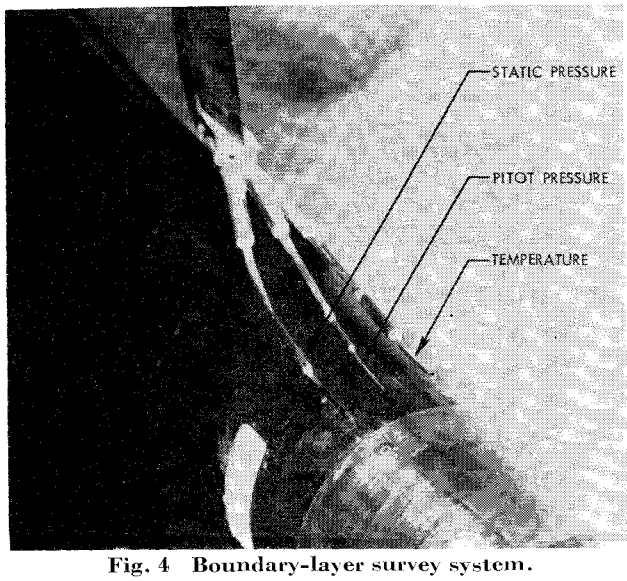

Fig. 4 Boundary-layer survey system.

of the models because of the more rapidly varying pressures and Mach numbers relative to the upstream end. The movable boundary-layer survey system (Fig. 4) consisted of three probes: total pressure, total temperature, and static pressure, mounted on a strut attached to a mechanism that provided vertical translation as well as angular rotation in the vertical plane. Thus, measurements could be made at numerous points throughout the boundary layer while the probes were essentially aligned with the surface of the model when surveys were being made.

The measuring of total pressure and total temperature in the boundary layer by means of the movable probe system was reasonably straightforward. Measurement of static pressures in the boundary layer, however, presented a real challenge. This measurement was complicated by the following factors: 1) the wall curvature of the models introduced substantial local stream angles (up to 12°), 2) interference between the probe support shock system and the probe boundary layer, and 3) unfavorable development of probe boundary layer associated with high Mach number and low Reynolds number. A substantial experimental effort, consisting of testing numerous static pressure probe and support configurations, was applied to this problem in the Lockheed and AEDC tunnels. As a result of this effort, a satisfactory static pressure probe configuration was evolved.

Another very challenging problem in this program involves the measurement of heat transfer. This problem is complex by virtue of the fact that, for models of a size appropriate for AEDC Tunnels A and B, the cooled model wall is relatively thin and the temperature drop across the wall is small over large portions of the model, particularly the upstream end where the heat-transfer rates are low. Accordingly, several techniques for measuring heat transfer were carefully explored. The solution to this problem consisted of developing a differential thermocouple for measuring the temperature drop across the cooled wall, as contrasted to measuring absolute temperature on both sides of the wall and calculating the difference. When the wall conductivity and thickness were known, the heat transfer was calculated using Fourier's law. Heat-transfer bench tests and wind-tunnel tests proved this to be a very accurate method of measuring heat transfer.

Experimental Data

Representative Mach number and static pressure distributions in the streamwise direction are shown in Fig. 5 for the Mach 8 design at a freestream Mach number of 8. The Mach number decreases significantly toward the downstream end of the model because of supersonic compressive turning.

Representative integrated characteristics of the boundary layer in terms of shape parameter and displacement thickness along the Mach 8 model at a freestream Mach number of 8 also are presented in Fig. 5. The shape parameter is the ratio of displacement thickness to momentum thickness. These two thickness parameters are obtained by integration of the boundary-layer velocity and density data. The shape parameter and displacement thickness decrease substantially as the boundary layer proceeds downstream in the adverse pressure gradients of the compression surface. This is, in general, due to 1) reductions in local Mach number with distance along the compression surface, and 2) improved velocity profiles in the lower Mach number regions.

It is of interest to determine the effects of heat transfer (cooling) on the boundary-layer characteristics in continuous adverse pressure gradients. First, however, it is worthwhile to examine the over-all heat-transfer characteristics of the cooled model with maximum cooling and adiabatic conditions. Representative heat-transfer rates and wall temperature distributions for the cooled model at freestream Mach number of 8 are shown in Fig. 6. It is noteworthy that an isothermal wall, in the streamwise direction, was obtained for both the maximum cooling as well as the adiabatic wall cases. The heat-transfer rates, although very small on the forward regions of the model wherein the

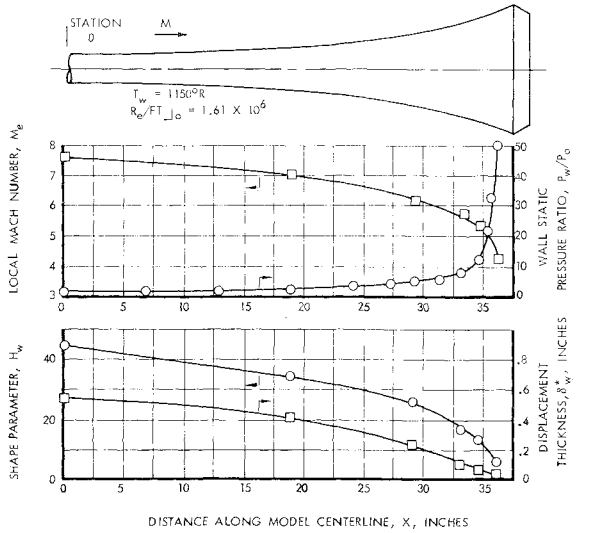

Fig. 5 Mach number, wall pressure, and boundary-layer characteristics on Mach 8 model, M_0 = 8.

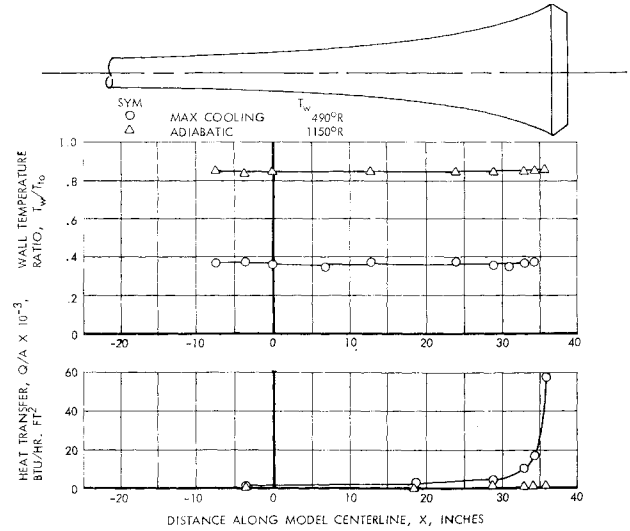

Fig. 6 Temperature and heat transfer along Mach 8 model, M_0 = 8.

Mach numbers are high, increased very rapidly in the downstream region of the model, where the Mach numbers are relatively low and streamwise gradients are high. This result can be explained by consideration of Stanton number and flow-per-unit-area variations with Mach number. For supersonic flow these parameters increase with reductions in Mach number; and the heat-transfer coefficient, which is proportional to these quantities, increases accordingly.

Representative effects of wall cooling on boundary-layer displacement thickness and velocity profile are shown in Fig. 7 for a freestream Mach number of 8.0. It is noted that although wall cooling produces significant favorable effects on the boundary layer in the relatively high Mach number forward regions of the model, the effects in the downstream low Mach number region are negligible. The absence of cooling effects is observed in both the displacement thickness and velocity profiles at the downstream end of the model (Fig. 7).

Analysis of the data indicates that this phenomenon is largely due to centrifugal force effects associated with wall curvature and a thicker initial boundary layer. This finding is substantiated by the data of Fig. 8, wherein the pressure distributions normal to the model wall are shown for both the cooled and adiabatic cases at two streamwise stations in the flow. The higher pressure gradients normal to the wall for the adiabatic relative to the cooled wall condition are a direct indication of stronger centrifugal force effects in the adiabatic case. This perhaps can be better understood when it is recalled that the pressure gradient across the boundary layer is approximately proportional to the ratio of boundary-layer thickness to radius of curvature. The boundary layer having the larger initial displacement thickness would, accordingly, be expected to have larger pressure gradients normal to the wall and correspondingly stronger centrifugal force effects, as observed in the adiabatic case.

It is of interest that the phenomenon discussed previously, involving initial differences in displacement thickness (at beginning of compression surface), which vanish at the downstream end of the model, also has been observed on the uncooled models in this research program under different test conditions than those of the cooled model. This has been found in cases where the displacement thickness at the beginning of the compression surface was larger because of 1) increases in freestream Mach number and 2) reductions in Reynolds number. In both of these cases, the differences in displacement thickness vanished by the time the flow reached the downstream end of the model, as shown in Fig. 9, in a manner similar to the behavior observed on the heat-transfer model. As in the cooled model tests, this finding has been

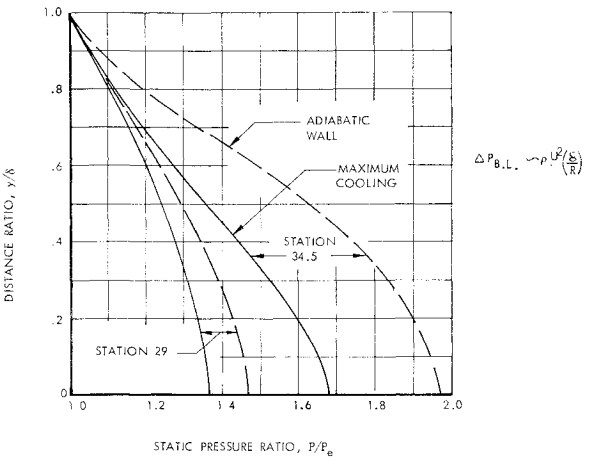

Fig. 8 Effects of cooling on static pressure profiles, $M_0 = 8$.

related to centrifugal force effects, as indicated by larger measured pressure gradients normal to the wall for the case of larger initial displacement thicknesses. Accordingly, it appears that in the freestream Mach number range of 4–8, for compression surfaces having curvatures of the magnitude of the models of this program, centrifugal force effects tend to predominate over cooling, Mach number, and Reynolds number for the range of variables in the present program. Although some exceptions to this might be found, it is clear that this powerful favorable phenomenon must be carefully considered in hypersonic inlet design and used to advantage where possible.

Theory

Two theoretical approaches have been developed in connection with this program. These are 1) the discontinuity/analogy and 2) the classical methods. The discontinuity/analogy method, described in Ref. 1, has been generalized in this paper to include pressure gradients normal to the wall. The method is described briefly below. The net distortion of the boundary layer in a continuous adverse pressure gradient is assumed to result from a combination of two simultaneous component actions at any streamwise station in the flow; one tends to distort the boundary layer and the other tends to restore it to a more uniform velocity profile. These two component actions are referred to as the distortion component and the restoring component, respectively. The method is illustrated qualitatively in

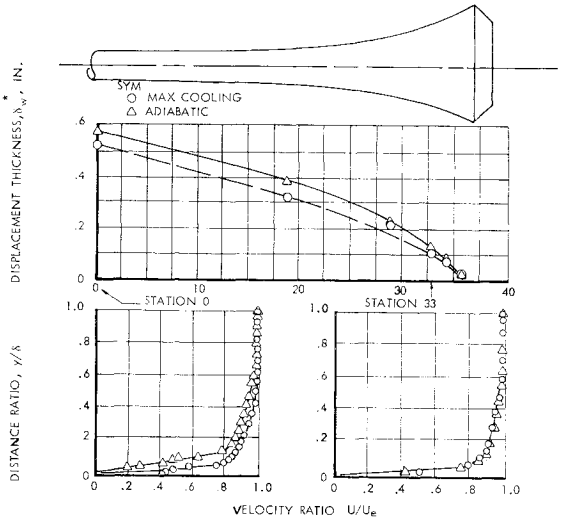

Fig. 7 Effects of cooling on displacement thickness and profile, $M_0 = 8$.

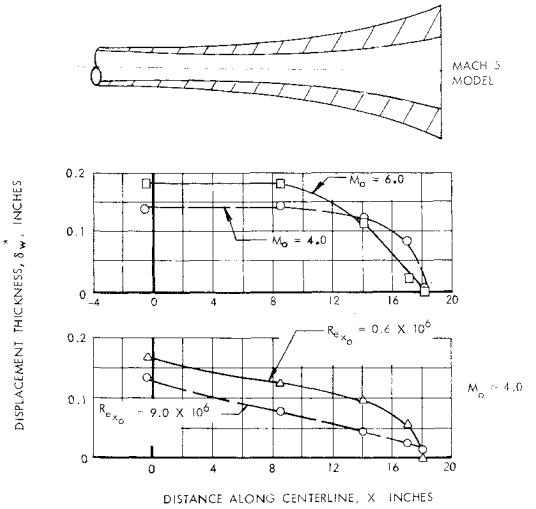

Fig. 9 Effects of Mach number and Reynolds number on displacement thickness.

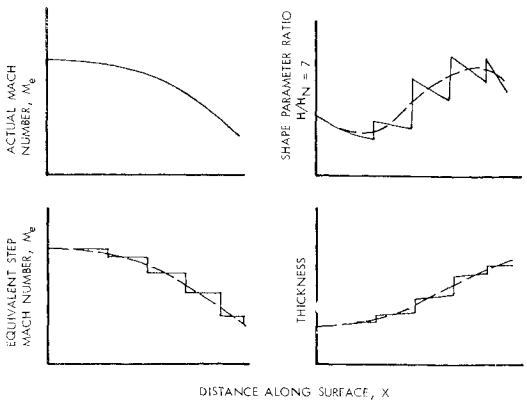

Fig. 10 Discontinuity/analogy method.

Fig. 10. In a continuous supersonic compression, the Mach number distribution is approximated by a series of steps. The discontinuities in Mach number give rise to discontinuities in shape parameter, representing the distortion component. The constant Mach number elements between discontinuities give rise to a relaxation (reduction) in shape parameter representing the restoring component. The basic conservation laws are applied in calculating both the distortion and restoring components. A more detailed description of the method is presented in the Appendix of this paper.

In the classical method, the boundary-layer characteristics are calculated utilizing a system of equations based on the conservation laws. These equations are solved simultaneously in conjunction with appropriate skin-friction, heat-transfer, and turbulent stress correlations. Results to date indicate good agreement between the two theories.

Correlation of Theory and Experiment

A correlation between the discontinuity/analogy theory and experimental data obtained in AEDC Wind Tunnels A and B has been made. In Figs. 11–14, representative results are shown in terms of shape parameter and displacement thickness for the Mach 8 model with and without heat transfer, at freestream Mach numbers of 6 and 8. As indicated in these figures, the theoretical results are generally in good agreement with the experimental data.

In the correlations just discussed, the attempt was made to match shape parameter and displacement thickness at the beginning of the compression surface. In addition, the boundary conditions at both the wall and the edge of the boundary layer were satisfied, namely, 1) the theoretical and experimental temperatures were matched at the wall and edge of the boundary layer, 2) the stagnation temperature

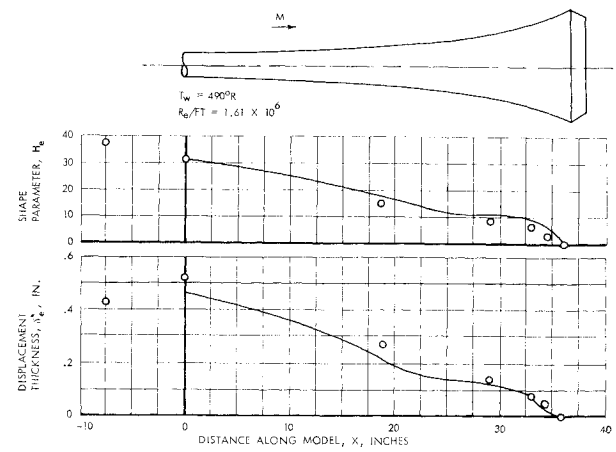

Fig. 12 Correlation of theory and experimental data, maximum cooling, $M_0 = 8$.

gradient at the edge was assumed zero, and 3) the velocity was assumed zero at the wall and the local freestream value at the edge. In attempting to match theoretical and experimental values of displacement thickness, theoretical temperature distributions through the boundary layer, as previously suggested, did not permit an appropriate match to be accomplished. Accordingly, it was necessary to develop a new total temperature profile in the present correlation. The profile adopted is written

$$T_t/T_{t_0} = T_w/T_{t_0} + [d + 2(1 - T_w/T_{t_0})]y/\delta + [-2d + (T_w/T_{t_0} - 1)](y/\delta)^2 + d(y/\delta)^3$$

The results, when applied in conjunction with a power law velocity profile, generally enabled a simultaneous matching of theoretical and experimental values of shape parameter, displacement thickness, velocity distribution, and stagnation temperature distribution through the boundary layer.

In some cases, however, it was found that although matching of theoretical and experimental values of shape parameter and displacement thickness could be achieved, utilizing the foregoing assumptions, theoretical and experimental temperature, and velocity profiles would not always match. An example of this problem is illustrated in Fig. 15 wherein the theoretical and experimental distributions of temperature and velocity are presented. These distributions correspond to the condition of matched theoretical and experimental values of shape parameter and displacement thickness. As indicated in the left-hand side of Fig. 15, it was necessary in some cases to distort the temperature profile in order to achieve matching values of shape parameter and displacement thickness. This is believed to be a result of an in-

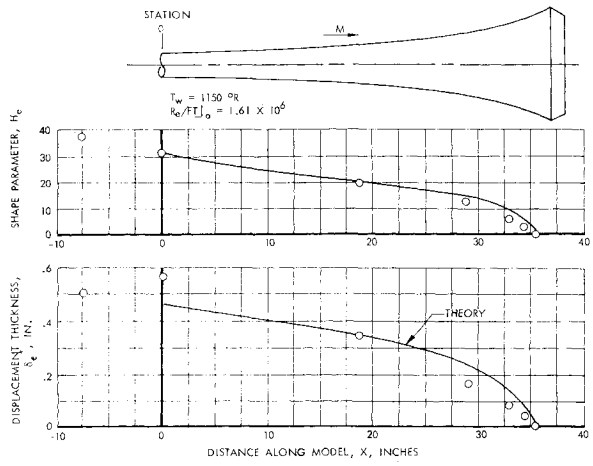

Fig. 11 Correlation of theory and experimental data, adiabatic wall, $M_0 = 8$.

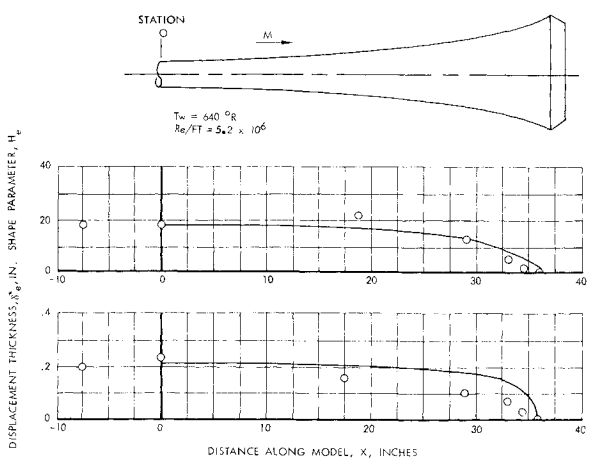

Fig. 13 Correlation of theory and experimental data, adiabatic wall, $M_0 = 6$.

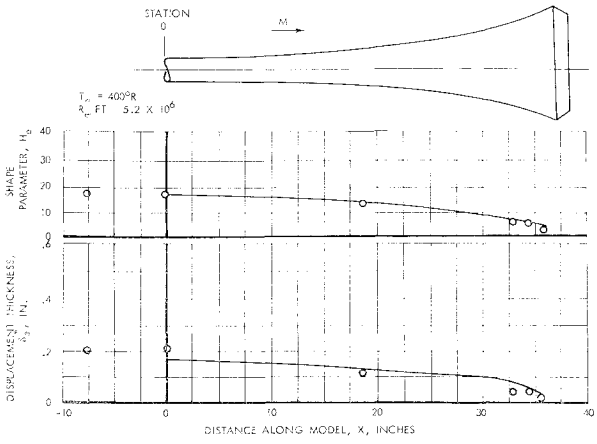

Fig. 14 Correlation of theory and experimental data, maximum cooling, $M_0 = 6$.

adequacy of the assumed power law velocity profile to describe the boundary layer in all cases. It is evident, for example, that, although the power law profile describes the major portion of the boundary layer in the left-hand part of Fig. 15, it fails to describe the profile with sufficient accuracy in the lower portion of the layer.

In other cases, the simultaneous matching of theoretical values of shape parameter, displacement thickness, temperature distribution, and velocity distribution was excellent as shown at the right-hand side of Fig. 15. In any event, it would be desirable to conduct additional analytical studies in an attempt to enable better matching of the various boundary-layer properties discussed previously. These studies would involve determination of improved theoretical representations of both stagnation temperature and velocity profiles through the boundary layer.

Applications

The objective of the present program is development of analytical methods for predicting boundary layers in the complex environment of hypersonic inlets. Accordingly, it is believed of interest to discuss briefly some examples illustrating applications of methods developed to date.

The inlets of these examples consist of a family of external compression inlets and one mixed compression inlet as shown in Fig. 16. The supersonic diffuser fineness ratio covers the range of approximately 1.5–5.0. Supersonic diffuser fineness ratio is defined as length of the external compression surface divided by inlet entrance diameter for external compression inlets. Fineness ratio of the mixed compression inlet is defined as length of the spike (up to the throat) plus

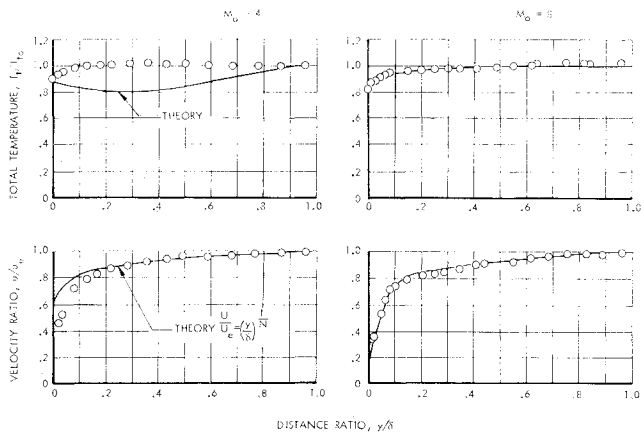

Fig. 15 Theoretical and experimental temperature and velocity distributions, H and δ^* matched.

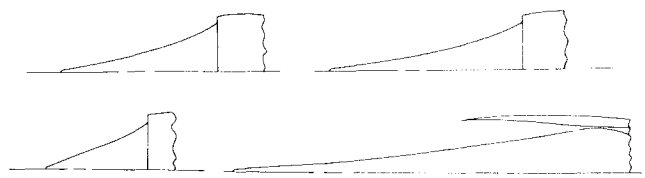

Fig. 16 Mach 8 inlets studied.

length of the cowl to the same station, divided by inlet entrance diameter.

The estimated distribution of shock-wave and boundary-layer losses is shown in Fig. 17 for a flight Mach number of 8.0 for the range of inlet fineness ratios studied. As would be expected, shock losses are much higher for low fineness ratio inlets relative to high fineness ratio inlets. Conversely, boundary-layer losses are much lower for low fineness ratio inlets relative to high fineness ratio inlets. Boundary-layer losses are presented with and without wall cooling and centrifugal force effects. The inlet surfaces were assumed to be cooled to 2000°F. Combined cooling and centrifugal force phenomena introduce major improvements in inlet pressure recovery, as indicated in Fig. 17. Centrifugal force effects are more pronounced in low fineness ratio inlets, whereas heat-transfer effects tend to predominate in high fineness ratio inlets.

It is noteworthy that the estimated net inlet pressure recovery, with heat-transfer and centrifugal force effects accounted for, maximizes at an inlet fineness ratio of approximately 3. When weight is considered in addition to pressure recovery, it would appear that an inlet in the fineness ratio range of 2 to 3 would represent a reasonable compromise.

Conclusions

In the experimental area of this program, one of the major problems involved measurement of heat transfer. This problem was encountered as a result of relatively thin model walls, imposed by scale limitations, combined with a small temperature drop across the wall. The solution consisted of developing a differential thermocouple for measuring the temperature drop directly, as contrasted with measuring absolute temperatures on both sides of the wall. Bench tests and wind-tunnel tests proved this to be a very accurate method of measuring heat transfer.

It was found from the experimental data in this program, for the range of variables tested, that centrifugal force effects associated with wall curvature tend to predominate over cooling, Mach number, and Reynolds number effects. This powerful phenomenon should be carefully considered in hypersonic inlet design and used to advantage wherever possible.

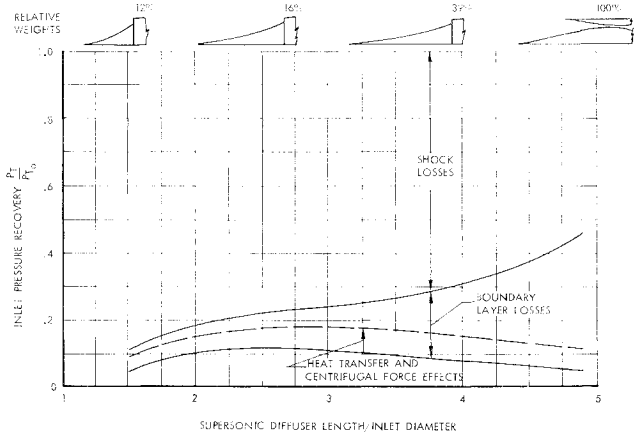

Fig. 17 Heat-transfer and centrifugal force effects on inlet performance, $M_0 = 8$.

A theory developed as part of this research effort was correlated with experimental data and agreement was generally good for both adiabatic and cooled wall conditions. Analysis indicated, however, that additional studies are desirable to obtain improved theoretical representations of both stagnation temperature and velocity profiles through the boundary layer.

Appendix: General Discontinuity/Analogy Procedure with Pressure Gradient Normal to the Wall

A general discontinuity/analogy procedure for treating a turbulent boundary layer with pressure gradient normal to the wall is described in this section. As discussed in the text, the method is comprised of two simultaneous component actions at any streamwise station in the flow, one tending to distort the boundary layer and the other tending to restore it to a more uniform flow. The detailed equations for the restoring and distortion components are presented below.

Restoring Component

At the initial station x_i, the boundary-layer thickness δ_i, displacement thickness δ_i^*, and form factor H_i are to be given, as well as a bivariant table of $P(x, y)$ and the values of total temperature T_{t_o}, wall temperature T_w, total pressure P_{t_o}, and local Mach number $M_e(x)$.

The following boundary-layer profiles are used:

Velocity profile

$$u/u_e = (y/\delta)^m \tag{A1}$$

Density profile

$$\rho/\rho_e = (T_e/T)(P/P_e) \tag{A2}$$

Temperature profile

$$\frac{T}{T_e} = \frac{h_w}{h_e} + \left[1 - \frac{CU_e^2}{H_e^*}\right]\frac{H_e^*}{h_e}\frac{u}{u_e} + \left[\frac{CU_e^2}{H_e^*} - \frac{U_e^2}{2H_e^*}\right]\frac{H_e^*}{h_e}\left(\frac{u}{u_e}\right)^2 \tag{A3}$$

The following integral parameters are defined:

$$\delta^* = \int_0^\delta (1 - \rho u/\rho_e u_e)dy \tag{A4}$$

$$\theta = \int_0^\delta (\rho u/\rho_e u_e)(1 - u/u_e)dy \tag{A5}$$

$$H = \delta^*/\theta \tag{A6}$$

Then the profile parameters m and CU_e^2/H_e^* are found such that the given initial values of δ_i, δ_i^*, and H_i are satisfied. The initial energy thickness ϕ_i is computed as follows:

$$\phi_i = \int_0^\delta \frac{\rho u}{\rho_e u_e}\left(1 - \frac{H^*}{H_e^*}\right)dy \tag{A7}$$

The effective Reynolds numbers Re_{eff_i} and $Re_{\mathrm{eff}_{i+1}}$, distances x_{eff_i} and $x_{\mathrm{eff}_{i+1}}$, and power law exponent m_{i+1} are found as previously (see Ref. 1). The skin friction is computed using Sivells and Payne correlation,[3]

$$C_{f_{i-(i+1)}} = \frac{0.088(\log \bar{R}_e' - 2.3686)\rho'/\rho_e}{(\log \bar{R}_e' - 1.5)^3} \tag{A8}$$

where

$$\overline{R_e'} = (R_{e_i}' + R_{e_{i+1}}')/2$$

and prime indicates conditions evaluated at the reference temperature.[3]

Now, from the momentum and energy equations,

$$\theta_{i+1} = \theta_i + \tfrac{1}{2}C_{f_{i-(i+1)}}\Delta X_{i-(i+1)} \tag{A9}$$

$$\phi_{i+1} = \phi_i + \tfrac{1}{2}C_{f_{i-(i+1)}}\left\{1 - \tfrac{1}{2}\left[\left(\frac{CU_e^2}{H_e^*}\right)_i + \left(\frac{CU_e^2}{H_e^*}\right)_{i+1}\right]\right\}\frac{\Delta x_{i-(i+1)}}{Pr^{2/3}} \tag{A10}$$

The parameters δ_{i+1} and $(CU_e^2/H_e^*)_{i+1}$ are found by satisfying Eqs. (A5, A7, A9, and A10).

Distortion Component

In the distortion (discontinuity) component, the values m_{i+1}, δ_{i+1}, $[CU_e^2/H_e^*]_{i+1}$, θ_{i+1}, and ϕ_{i+1} are known at x_{i+1} just upstream of the discontinuity. The parameters m_{i+2} $\delta_{(i+2)}$ and $[CU_e^2/H_e^*]_{(i+2)}$ are then found such that the following conservation equations are satisfied:

Energy equation across discontinuity

$$(\rho_e U_e \phi)_{i+1} = (\rho_e U_e \phi)_{i+2} \tag{A11}$$

Momentum equation across discontinuity

$$\left(\frac{\delta^*}{\theta}\right)_{i+2} = \frac{2\frac{\delta_{i+2}}{\delta_{i+1}}\cdot\frac{q_{e_{i+2}}}{P_{e_{i+1}}}\left(\frac{\delta^*}{\delta}\right)_{i+2}}{\left[\begin{array}{l} 2\frac{\delta_{i+2}}{\delta_{i+1}}\frac{q_{e_{i+2}}}{P_{e_{i+1}}}\left[1 - \left(\frac{\delta^*}{\delta}\right)_{i+2}\right] - \\ 2\frac{q_{e_{i+1}}}{P_{e_{i+1}}}\left[1 - \left(\frac{\delta^*}{\delta}\right)_{i+1} - \left(\frac{\theta}{\delta}\right)_{i+1}\right] + \\ \frac{1}{2}\left[1 - \frac{\delta_{i+2}}{\delta_{i+1}}\right]\left[1 + \frac{P_{e_{i+2}}}{P_{e_{i+1}}}\right] - \\ \frac{\bar{P}_{i+1}}{P_{e_{i+1}}} + \frac{\bar{P}_{i+2}}{P_{e_{i+1}}}\frac{\delta_{i+2}}{\delta_{i+1}} \end{array}\right]} \tag{A12}$$

Considering continuity across a discontinuity,

$$\delta_{i+2} = \frac{(\rho_e u_e)_{i+1}}{(\rho_e u_e)_{i+2}}\delta_{i+1}\left[\frac{1 - (\delta^*/\delta)_{i+1}}{1 - (\delta^*/\delta)_{i+2}}\right] \tag{A13}$$

When these equations are satisfied, the conditions downstream of the discontinuity are known. The procedure for the next restoring component, following the discontinuity, is repeated. In the complete solution, comprised of a series of discontinuity and restoring components, the procedures outlined previously are repeated until the end of the compression surface is reached. It has been found that 40–60 increments are sufficient for a typical hypersonic inlet.

References

[1] Stroud, J. F. and Coleman, D. M., "Hypersonic inlet boundary-layer prediction," ARS J. **32**, 733–738 (1962).

[2] Stroud, J. F. and Miller, L. D., "Hypersonic inlet boundary-layers," AIAA Preprint 65-605 (1964).

[3] Sivells, J. C. and Payne, R. G., "A method of calculating turbulent boundary layer growth at hypersonic Mach numbers," Arnold Engineering Development Center TR 59-3 (1959).